

**DEVELOPMENT AND ANALYSIS OF LINEAR
RESONANT SCANNER WITH TORSIONAL
MECHANISM**

KOAY LOKE KEAN

UNIVERSITI SAINS MALAYSIA

2013

**DEVELOPMENT AND ANALYSIS OF LINEAR
RESONANT SCANNER WITH TORSIONAL
MECHANISM**

BY

KOAY LOKE KEAN

**Thesis submitted in fulfillment of the
requirements for the degree of
Doctor of Philosophy**

July 2013

DEDICATION

This thesis is dedicated to my family, who offered me unconditional love and support throughout the course of my PhD thesis. For the USM Vice-Chancellor, who offered me prestigious financial support in the form of Vice-Chancellor Award.

ACKNOWLEDGEMENT

First of all, I would like to reserve my sincere thanks to my supervisors, Professor Horizon Walker Gitano-Briggs and Professor Mani Maran Ratnam, for supporting me during these past three and half years. Professor Horizon Walker Gitano-Briggs provided insightful discussions about the research, he also giving me a large freedom to pursue various researches without objection. I would like to thank for Professor Mani Maran Ratnam. I hope I could be as energetic, passionate as Professor Mani Maran Ratnam, and to be able to command the audience as well as he did someday. He is my resource for helping me crank out this thesis. A special thanks to Professor Mani Maran Ratnam on providing expert advices on the journal writing.

I would like to thank for Dr Khoo Bee Ee, Dr. Chan Keng Wai and Dr.-Ing Muhammad Razi bin Abdul Rahman who gave me confidence, care and concern for my research work. Their constant support, encouragement has become a source of inspiration for me. I would like to forward special thanks to my fellow colleagues, Khoo Aik Soon, Vigren Radha, and Chuah Han Guan for their support and help during my post graduate studies.

A good support system is crucial in surviving and crank out the research products in my research work. I was lucky to have the support from the technicians, especially Ms. Baharom Awang. He is a very helpful and high efficient staff. Above all, I would like to express my deepest gratitude to the government of Malaysia and USM for awarding my Postgraduate Research Grant Scheme and Vice-chancellor Award which relieved me of financial insecurity.

TABLE OF CONTENTS

DEDICATION	ii
ACKNOWLEDGEMENT	iii
TABLE OF CONTENTS	iv
LIST OF FIGURES	xi
LIST OF TABLES	xxiii
LIST OF ABBREVIATION	xxiv
LIST OF SYMBOL	xxvi
ABSTRAK	xxvii
ABSTRACT	xxix
CHAPTER 1 INTRODUCTION	1
1.0 Research background	1
1.1 Problem statement	12
1.2 Objectives	13
1.3 Scope of study	14
1.4 Thesis outline	15
CHAPTER 2 LITERATURE REVIEW	17
2.0 Introduction	17
2.1 Overview of optical scanning technology	18

2.1.1	Polygonal scanner	18
2.1.2	Holographic scanner	21
2.1.3	Oscillatory resonant scanner	23
2.2	Actuators	26
2.2.1	Galvanometric actuator	26
2.2.2	Piezoelectric actuator	29
2.2.3	Voice coil motor	32
2.3	Compliant structure	33
2.3.1	Flexure hinge	34
2.3.2	Cantilever spring	36
2.3.3	Torsional spring	38
2.4	Summary of the optical scanner technology	43
2.5	Control system	45
2.5.1	Hysterical frequency response	46
2.6	Damping characteristic of linear optical scanner	49
2.7	Applications of linear optical scanner (LOS)	52
2.8	Summary	54
CHAPTER 3 SCANNER DESIGN AND GEOMETRIC STUDY ON TORSIONAL SPRING		56

3.0	Overview	56
3.1	Design considerations	57
3.2	Conceptual design	60
3.3	Conceptual design modeling	62
3.4	Preliminary scanner design	65
3.4.1	Mechanical design	65
3.4.2	Circuit design.....	68
3.5	Torsional spring design	70
3.5.1	Finite element model	74
3.5.2	Optimization study algorithm	77
3.5.3	Results and discussion for the FEA results	78
	3.5.3 (a) Experimental- simulation validation.....	79
	3.5.3 (b) Stress level theory.....	80
	3.5.3 (c) Geometric study.....	82
	3.5.3 (d) Optimized torsional spring	89
3.6	Summary	92
CHAPTER 4 VOICE COIL MOTOR DEVELOPMENT		93
4.0	Overview	93
4.0.1	Suspended plate design.....	94

4.0.2	Voice coil motor design.....	97
4.1	Air core coil design	100
4.1.1	Theoretical formulation of magnetic force	100
4.1.2	Air core coil constraint	104
4.1.3	Experimental setup	108
4.1.4	Results and discussion	111
	4.1.4 (a) Analytical results and experimental results for ACC	
	Model 1	112
	4.1.4 (b) Analytical results and experimental results for ACC	
	Model 2	115
	4.1.4 (c) Analytical results and experimental results for ACC	
	Model 3	115
	4.1.4 (d) Analytical results and experimental results for ACC	
	Model 4	119
4.2	Magnet position considerations	121
4.2.1	Theory on resonant scanner vibration.....	123
4.2.2	Analysis of the relationship between magnet positions and scanner characteristics	130
4.2.3	Experimental-simulation validation for magnet position	134
4.2.4	First FEA results	135

4.2.4 (a) Resonant frequency	135
4.2.4 (b) Angular displacement.....	136
4.2.4 (c) Stress level.....	137
4.2.5 Second FEA results for magnet position selection.....	138
4.3 Summary	142
CHAPTER 5 SCANNER DAMPING CHARACTERISTICS	144
5.0 Overview	144
5.1 Introduction of the nonlinear damping.....	145
5.1.1 Theory of exponential damping model for free response profile prediction	146
5.2 Methodology	149
5.2.1 Experimental setup	149
5.2.2 Nonlinear damping model development algorithm	151
5.2.3 Nonlinear damping model	153
5.2.4 Experimental-numerical validation	158
5.3 Numerical study on various natural frequency and damping ratio	159
5.3.1 Natural frequency variation	160
5.3.2 Damping ratio variation.....	161
5.4 Case studies on damping characteristics	163

5.4.1	Comparison of the free response profile with pressure variations on rigidly mounted scanner and spring demounted scanner	165
5.4.2	Comparison of the free response profile with pressure variations and different dampers	169
5.4.3	Comparison of the free response profile with pressure variation on the rigidly mounted scanner and scanner mounted with hard rubber damper.....	173
5.5	Summary	175
CHAPTER 6 TEST ALGORITHMS AND PERFORMANCE OF SCANNER .		178
6.0	Overview	178
6.1	Algorithms for performance testing.....	179
6.2	Methodology	183
6.2.1	Resonant frequency detection.....	183
6.2.2	Hysterical frequency response detection	190
6.3	Results and discussion	193
6.3.1	Frequency perturbation.....	194
6.3.2	Laser scan line length control.....	196
6.3.3	Hysterical frequency response	199
6.4	Summary	202

CHAPTER 7 CONCLUSIONS AND FUTURE WORK.....	204
7.0 Conclusions.....	204
7.1 Research contributions.....	206
7.2 Recommendation for future work.....	207
REFERENCES.....	209
APPENDICES.....	232
LIST OF PUBLICATIONS.....	237
LIST OF AWARDS.....	237

LIST OF FIGURES

Figure 1.1: Frame forms of tracking and aiming	3
Figure 1.2: Vibration mode of cantilever spring	7
Figure 1.3: Typical MEMS torsional scanner (Mu et al., 2008)	9
Figure 2.1: Overview of literature review	17
Figure 2.2: Classification of rotational scanner (Leo, 2003)	18
Figure 2.3: Pyramidal polygon and prismatic polygon (Leo, 2003)	20
Figure 2.4: Typical holographic scanner (Rowe, 1997)	22
Figure 2.5: (a) Rotary scanner, prismatic polygon scanner consist of multiple mirrors (b) Oscillatory scanner, single mirror reflection.....	25
Figure 2.6: Moving iron type galvo (Aylward, 2003).....	27
Figure 2.7: Moving coil type galvo (Aylward, 2003)	28
Figure 2.8: Moving magnet type galvo (Aylward, 2003)	29
Figure 2.9: The thin curved beam device obtained with a pseudo-rigid-body model from finite element analysis. (Chen et al., 2010a).....	30
Figure 2.10: Design of the tip-tilt actuator (a) Structure of the scanner assembly and (b) Operation principle of the laser scanner (Xiang et al., 2010).....	31
Figure 2.11: Schematic diagram of voice coil motor (Youm et al., 2007)	32

Figure 2.12: Scanner with voice coil motors and compliant structure (Qingkun et al., 2008).....	33
Figure 2.13: Flexure hinge (Qingkun et al., 2008).....	35
Figure 2.14: Scheme of spherical hinge laser scanner (He et al., 2006).....	36
Figure 2.15: Cantilever spring scanner (Kheng et al., 2010).....	37
Figure 2.16: Mechanical rotation of 11.8° has been attained at a magnetic field of 3.5 mT (Garnier et al., 2000).	38
Figure 2.17: (a) Uniaxial mechanical resonant scanner (MRS) (b) Biaxial MEMS scanner (Urey, 2002)	40
Figure 2.18: (a) Picture of a full die (b) Detail of inner and outer flexures and comb drive (Arslan et al., 2010)	42
Figure 2.19: Torsional spring micro-scanner (Tang and Fang, 2011)	43
Figure 2.20: Typical hysterical frequency response of the torsional scanner (Arslan et al., 2010)	47
Figure 2.21: Hysterical frequency response of the rectangular beam (Garnier et al., 2000)	48
Figure 2.22: Hysterical frequency response of the torsional hinge (Miyajima et al., 2005)	49
Figure 3.1: The phases in mechanical design for large scale resonant scanner in Chapter 3	57
Figure 3.2: Conceptual modelling of linear optical scanner's holder.....	62

Figure 3.3: Product envelope of the scanner	63
Figure 3.4: Modelling of torsional spring: (a) Without suspended plate (b) With suspended plate.....	64
Figure 3.5: Suspended plate fastened to the torsional spring by (a) the rivets (b) screws and nuts	64
Figure 3.6: Torsional spring and device components of preliminary scanner	66
Figure 3.7: Angular displacement of the mirror-spring at extremity of motion (plan view)	66
Figure 3.8: Peak-to-peak deflection of the suspended plate versus the distance between the coil and the permanent magnet measured for drive current of 0.15A.....	67
Figure 3.9: Experimental setup	68
Figure 3.10: Coil voltage and the photodiode voltage/ position sensor voltage	69
Figure 3.11: Arduino Atmega 328p	70
Figure 3.12: ‘Extended’ printed circuit board (PCB) for Arduino FSM rev1.1 soldered with the electronic components	70
Figure 3.13: Light pattern (a) static (b) during scanning	73
Figure 3.14: Microscopic view of a failure. Length of the torsional spring is in the lateral direction. Notice the crack propagating vertically (downward to upward), 2000× magnification	73

Figure 3.15: Schematic showing the twist axis and the displacement distribution in the torsional spring, suspended plate and magnet	75
Figure 3.16: A portion of the FEA model showing the 3D mesh of the torsional spring, suspended plate and magnet	75
Figure 3.17: Mode shapes of the torsional spring oscillation: (a) Mode shape 1: 43.53 Hz (b) Mode shape 2: 77.83 Hz (c) Mode shape 3: 275.20 Hz (d) Mode shape 4: 1358.50 Hz (e) Mode shape 5: 1587.80 Hz	76
Figure 3.18: Flowchart for simulation methodology with the condition only one of the dimensions is independent variable. In this flowchart, length was used as the independent variable.....	78
Figure 3.19: Experimental results: angular displacement versus driving frequency of the scanner when torsional spring in the preliminary scanner is used	79
Figure 3.20: Stress distribution of torsional spring in the preliminary scanner. Maximum stress is 0.72 GPa located at the tip of the screw hole	80
Figure 3.21: Maximum stress versus width	83
Figure 3.22: Maximum stress versus thickness.....	85
Figure 3.23: Maximum stress versus length	86
Figure 3.24: Sensitivity ratio versus % change in dimension	87

Figure 3.25: Flowchart for simulation methodology with the condition width and thickness are independent variable	88
Figure 3.26: Stress versus change width and thickness at constant length	89
Figure 3.27: (a) Worst case spring with a maximum stress of 0.90 GPa. (b) Optimized spring with maximum stress of 0.63 GPa.....	91
Figure 4.1: The electromagnetic system designs for large scale resonant scanner in Chapter 4	94
Figure 4.2: Suspended plate designs: (a) Preliminary scanner design (b) Modified design.....	95
Figure 4.3: Plan view of the suspended plate designs: (a) Preliminary scanner design (b) Modified scanner design	96
Figure 4.4: FEA model for modified suspended plate, first mode resonant frequency 40.23 Hz	97
Figure 4.5: Voice coil motor (VCM): (a) Load speaker with VCM (b) Structure of VCM (Jiang et al., 2012)	99
Figure 4.6: B-H Curve of neodymium magnet (Ulaby, 2001).....	100
Figure 4.7: Schematic of air core coil (Jung and Baek, 2002).....	101
Figure 4.8: Product envelope (plan view)	103
Figure 4.9: Air core coils: (a)With bobbin (b) Without bobbin.....	107
Figure 4.10: Experimental setup to measure magnetic force: (a) Photograph of the setup (b) Schematic diagram of the setup	110

Figure 4.11: Torque arm of the “L” bar	111
Figure 4.12: Cross-sectioned of ACC, position 2 is zero of distance from magnet to ACC, position 1 is negative region and position 3 is positive region	112
Figure 4.13: Magnetic force between coil and magnet versus distance from magnet for Model 1 for both bobbin and without bobbin ACC.....	113
Figure 4.14: Magnetic force between coil and magnet versus distance from magnet for Model 2	117
Figure 4.15: Magnetic force between coil and magnet versus distance from magnet for Model 3	118
Figure 4.16: Magnetic force between coil and magnet versus distance from magnet for Model 4	120
Figure 4.17: Schematic of suspended plate (plan view)	122
Figure 4.18: Twist axis, displacement angle θ , and length l of the torsional spring	123
Figure 4.19: Angular displacement versus time for free vibration motion of the system when a small angular displacement of 4° was displaced	125
Figure 4.20: Maximum positive value of angular displacement versus time for free vibration motion of the system	126
Figure 4.21: The width and the mass for the partitions of suspended plate and magnets,; (a) Top view (b) Isometric view.....	128

Figure 4.22: Positions of magnets on the suspended plate.....	131
Figure 4.23: Flowchart for first FEA methodology with the condition of the forces applied to magnet position 2 and 3 were the same with the force applied to magnet position 1	132
Figure 4.24: Flowchart for second FEA methodology with the conditions: width and force were allowed for varying.....	133
Figure 4.25: Natural frequency variation of the scanner with distance of the magnet from the twist axis	134
Figure 4.26: ω/ω_0 versus distance from the axis	136
Figure 4.27: θ/θ_0 versus distance from the axis.....	136
Figure 4.28: σ/σ_0 versus distance from the axis	138
Figure 4.29: Stress versus various spring width for targeted frequency and angular displacement of 30°	139
Figure 4.30: Magnetic fields as imaged with MFVF	140
Figure 4.31: Vector Field Opera-13 results (a) Magnetic field among two magnets when they are side by side to each other (b) Magnetic field among two magnets when they are apart from each other.....	141
Figure 5.1: Components of scanner prototype	144
Figure 5.2: General free response of an underdamped oscillation system (Balachandran and Magrab, 2004)	148
Figure 5.3: Experimental setup	150

Figure 5.4: Displacement sensor calibration curve	150
Figure 5.5: Overview flowchart for piece-wise method used in obtaining the nonlinear damping ratio function	152
Figure 5.6: Free response profile obtained experimentally and maxima curve of the oscillation	153
Figure 5.7: Damping ratio versus angular displacement.....	154
Figure 5.8: Numerical and experimental free response profiles and amplitude ratio of experimental numerical profile.....	155
Figure 5.9: Piece-wise damping ratio versus time	156
Figure 5.10: Free response profile of experimental and time dependent damping ratio model.....	156
Figure 5.11: Nonlinear damping ratio versus angular displacement.....	157
Figure 5.12: Maxima curves of the linear, nonlinear damping models, experimental result. Amplitude ratio of experimental result to nonlinear model results shown in dash-dot line	158
Figure 5.13: Modeled free response profile for resonant frequencies of 40.0 Hz and 38.5 Hz, dashed line is the amplitude ratio curve	161
Figure 5.14: Modeled free response profile for damping ratios of 0.00152 and 0.00142 at 40.0 Hz, dashed line is the amplitude ratio curve	162
Figure 5.15: Demounted setup: The scanner is suspended from a soft spring.....	164

Figure 5.16: (a) Polyurethane Soft Foam (b) Rubber Damper	165
Figure 5.17: (a) Free response of the rigidly mounted scanner for vacuum pressure (resonant frequency of 40.0 Hz) and ambient pressure (resonant frequency of 40.0 Hz), dashed line is the amplitude ratio curve. (b) Free response of the spring demounted scanner for vacuum pressure (resonant frequency of 38.5 Hz) and ambient pressure (resonant frequency of 38.5 Hz), dashed line is the amplitude ratio curve	166
Figure 5.18: (a) Free response of the spring demounted scanner (resonant frequency of 38.5 Hz) and rigidly mounted scanner (resonant frequency of 40.0 Hz) for ambient pressure, dashed line is the amplitude ratio curve (b) Free response of the spring demounted scanner (resonant frequency of 38.5 Hz) and rigidly mounted scanner (resonant frequency of 40.0 Hz) for vacuum pressure, dashed line is the amplitude ratio curve	167
Figure 5.19: (a) Scanner rigidly mounted to the chamber with infinite mass (b) Scanner demounted by soft spring where $k'' \ll k'$	168
Figure 5.20: Free response of the scanner with rubber damper for vacuum pressure (resonant frequency of 38.5 Hz) and ambient pressure (resonant frequency of 38.5 Hz), dashed line is the amplitude ratio curve. (b) Free response of the scanner with PU soft for vacuum pressure (resonant frequency of 38.5 Hz) and ambient pressure (resonant frequency of 38.5 Hz), dashed line is the amplitude ratio curve	170

Figure 5.21: Experimental setup to measure the displacement of PU soft in low pressure, z -axis is the measured displacement during expansion.....	171
Figure 5.22: “Swelling” displacement of PU soft versus pressure (positive displacement is expansion, negative displacement is contraction).....	172
Figure 5.23: (a) Free response of the scanner with rubber damper and PU soft for ambient pressure, dashed line is the amplitude ratio curve. (b) Free response of the scanner with rubber damper and PU soft for vacuum pressure, dashed line is the amplitude ratio curve.....	173
Figure 5.24: (a) Free response of rigidly mounted scanner (resonant frequency of 40.0 Hz) and scanner with rubber damper (resonant frequency of 38.5 Hz) for vacuum pressure, dashed line is the amplitude ratio curve. (b) Free response of rigidly mounted scanner (resonant frequency of 40.0 Hz) and rubber damper (resonant frequency of 38.5 Hz) for ambient pressure, dashed line is the amplitude ratio curve	175
Figure 6.1: Portion of the free vibration response for the scanner prototype with time interval from 0 s to 0.5 s.....	181
Figure 6.2: Experimental setup for resonant frequency tracking: (a) Schematic diagram (b) Photograph of the setup.....	184
Figure 6.3: Torsional spring scanner (a) plan view (b) side view.....	185

Figure 6.4: Free underdamped response profile when displaced by servo motor.....	186
Figure 6.5: Sensor voltage and Schmitt trigger voltage.....	186
Figure 6.6: Schematic diagram of the feedback control for resonant frequency detection	188
Figure 6.7: Light detection sensor voltage versus time.....	188
Figure 6.8: Flowchart of the algorithm for frequency re-tracking.....	189
Figure 6.9: Masses addition to the scanner	190
Figure 6.10: Constant scan width with various throw distances.....	191
Figure 6.11: Constant throw distance with various scan widths.....	191
Figure 6.12: Experimental setup for constant scan width when the throw distance is varied (a) Schematic diagram of the setup (b) Photograph of the setup	193
Figure 6.13: Angular displacement of the scanner versus time when mass 1 is added without LDR feedback	194
Figure 6.14: Resonant frequency versus time when mass addition	195
Figure 6.15: Angular displacement versus time when mass addition and after the feedback of changed resonant frequency	196
Figure 6.16: Scanning patterns: (a) Static (b) During scanning.....	196
Figure 6.17: Scan lines' length measurement from left to right	198

Figure 6.18: Normalized scan lines length with total length versus scanning length and inverse relationship for timing.....	198
Figure 6.19: Constant scan lines length scanning on a flat screen: (a) 2 scan lines (b) 3 scan lines	198
Figure 6.20: Captured scan images and threshold processed images at throw distance of 300 mm: (a) Scan width of 13 mm at 39 Hz (b) Scan width of 582.0 mm at 43 Hz.	199
Figure 6.21: Hysterical frequency response of torsional spring mechanism resonant scanner	200
Figure 6.22: Drive frequency versus throw distance when scan width is 582 mm.....	201
Figure 6.23: Scan width versus various throw distances for 5 tests	202

LIST OF TABLES

Table 1.1: Some applications of laser scanning technology (Leo, 2003)	2
Table 2.1: Summary of the optical scanner technology	44
Table 3.1: Design specification of the resonant scanner	60
Table 3.2: Design characteristics of the large scale resonant scanner	61
Table 3.3: Properties and dimensional constraints	71
Table 3.4: Properties of magnet and suspended plate	72
Table 4.1: Dimensions constraint of ACC	104
Table 4.2: Specification of coil model without bobbin, direct current=0.5 A	105
Table 4.3: Specification of coil model with bobbin, direct current=0.5 A	106
Table 4.4: Comparison of the magnetic force for various models with bobbin	121
Table 6.1: Summary of the function, rule-based and hardware required for testing algorithms	180
Table 6.2: Drive frequency needed to attain the constant scan width for various throw distances and the deviation from 582 mm	202

LIST OF ABBREVIATION

ABBREVIATION	DESCRIPTION
AC	Alternating Current
ACC	Air Core Coil
APA	Amplified Piezoelectric Actuator
CCD	Charge-coupled Device
CFF	Critical Flicker Frequency
CM	Compliant Mechanism
DAQ	Data acquisition system
DC	Direct Current
DoC	Degree of Constraint
DRIE	Deep Reactive Ion Etching
FEA	Finite Element Analysis
HEL	High Energy Laser System
LDR	Light Dependent Resistor, used as the light detection device
LED	Light Emitting Diode
Lidar	light detection and ranging
LOS	Linear Optical Scanner
MEMS	Microeletromechanical Systems
MFVF	Magnetic Field Viewer Film
MRS	Mechanical Resonant Scanner
MW	Molecular Weight
PCB	Printed Circuit Broad
PWM	Pulse Width Modulation

PU soft	Polyurethane soft foam
UVA	Ultraviolet A
UVB	Ultraviolet B
VCM	Voice Coil Motor
V_{pp}	Peak-to-peak Voltage
SWG	Standard Wire Gauge

LIST OF SYMBOL

SYMBOL	DESCRIPTION
B	Flux density
H	Magnetic field
σ_u	Ultimate tensile strength

PEMBANGUNAN DAN ANALISIS PENGIMBAS SALUNAN LELURUS DENGAN MEKANISMA PEGAS KILASAN

ABSTRAK

Saiz cermin yang lebih besar telah digunakan dalam pelbagai teknologi pengimbasan, seperti projektor lonjatan dekat, komunikasi optik ruang bebas dan pengimbas barkod. Pelbagai penyelidikan telah dijalankan pada saiz cermin besar dalam sistem mikroelektromekanikal (MEMS). Sebagai contoh, penyelidikan telah dijalankan pada mikromesin pengimbas polisilikon yang digunakan sebagai pengimbas barkod. Walau bagaimanapun, kelengkungan cermin yang terdapat dalam mikromesin pengimbas polisilikon telah menyebabkan imej terherot. Selain itu, voltan operasi yang tinggi juga menghalang penggunaan pengimbas jenis MEMS dalam aplikasi pegang-tangan. Dalam kajian ini, pengimbas salunan lurus yang terdiri daripada elektronik dipacu secara salunan dan bermekanisme pegas kilasan telah dibina untuk aplikasi paparan. Pembangunan pengimbas ini telah diklasifikasikan mengikut fungsi komponen, seperti struktur patuhan dan penggerak. Analisis unsur terhingga (FEA) telah digunakan untuk membina pegas kilasan yang terdapat dalam struktur compliant dan analisis pada parameter geometri pegas telah dijalankan. Pegas kilasan optimum dengan paras tegasan terendah telah dipilih sebagai rekabentuk terakhir. Penggerak yang terdiri daripada gegelung berterasan angin (ACC) telah digunakan; analisis geometri gegelung telah dijalankan untuk memaksimumkan daya magnetik. ACC dengan panjang minimum, jejari dalam minimum dan jejari luar maksimum telah digunakan. Selain itu, FEA pada pengimbas telah membuktikan bahawa frekuensi salunan, anjakan sudut dan paras tegasan adalah dipengaruhi oleh kedudukan magnet. Selepas pembangunan

pengimbas, prestasi pengimbas telah dikaji. Satu model redaman bukan lurus telah dibuktikan mampu menganalisa dan meramal profil sambutan bebas berdasarkan keputusan eksperimen. Model redaman juga membuktikan bahawa gangguan frekuensi berlaku semasa cagak pada pengimbas berubah. Sambutan frekuensi histeresis pada pengimbas salunan lurus adalah pertama kali dilaporkan dalam kajian ini. Selain itu, hubungan antara sudut imbasan dan frekuensi bukan sahaja telah digunakan untuk mencapai mekanik gandaan lebih penggunaan hubungan ini juga merupakan temuan baru. Pengimbas bercermin besar ini merupakan pengimbas bermekanisme pegas kilasan pertama yang mencapai sudut imbasan sebesar 87.1° dengan voltan 5 V.

DEVELOPMENT AND ANALYSIS OF LINEAR RESONANT SCANNER WITH TORSIONAL MECHANISM

ABSTRACT

Large size mirror scanners are needed in several scanning technologies such as, ultra short-throw projector, free-space optical communications and barcode scanner. Several researches on large size mirror in microelectromechanical systems (MEMS) scanner were conducted. For instance, research on micromachined polysilicon microscanners has been performed for barcode scanner. However, the curvature of the microscanners causes image distortion. Furthermore, high operation voltages of the MEMS scanner deter the usage of MEMS scanner in hand-held applications. In this research, a linear resonant scanner consisting of an electronically driven mechanically-resonant torsional spring-mirror system was developed for display applications. The scanner was designed according to the functional components such as compliant structure and actuator. The torsional spring which is the compliant structure was modeled with finite element analysis (FEA) and geometry studies were conducted. The optimized torsional spring with the lowest stress level was selected for the design. The actuator of air core coil (ACC) was used in the scanner; geometry study was used to maximize the magnetic forces of the ACC. The ACC of with minimum length, minimum inner radius and maximum outer radius was used. Besides, experimental analysis and FEA of the scanner showed that resonant frequency, angular displacement and stress level are affected by the magnet position on the suspended plate. After the scanner design, several characteristic studies were conducted. A nonlinear damping model is proven to be able to analyze and predict the free vibration response of the scanner based on experimental results.

The damping model is able to accommodate the frequency perturbation which happens when the scanner mounting is changed. The hysterical frequency response on the large scale torsional spring mechanism is first found in this research work. Furthermore, the relationship between scanning angle and driving frequency was employed for extra mechanical gain. The proposed resonant scanner extends the ability of the torsional mechanism scanner for large angular displacement of 87.1° with low voltage input of 5 V.

CHAPTER 1 INTRODUCTION

1.0 Research background

An optical scanner serves as a device to convert the information in a product into a signal. An example of such device is barcode scanner. Conversely, a scanner is also used as a device to construct an image from a series of signal impulses and display them onto a screen. Examples of such device include the projector and laser display scanner. In these ways, the optical scanner becomes an information encoder and decoder, thus serving as the key device for advanced information transfer.

Generally, scanning technology can be separated into two categories: laser scanning and remote sensing. The main difference between laser scanning and remote sensing is that in the laser scanning a laser is employed as the light source. Meanwhile, in remote sensing, the sensing of the light primarily in infrared spectrum from the objects is employed (Leo, 2003). An optical system comprising of mirror and lens to control the laser beam is needed in laser scanning, while remote sensing systems do not required the optical systems when capturing the radiant flux from the objects (Leo, 2003). Table 1.1 shows the applications of laser scanning technology after the arrangement by Leo (2003).

Table 1.1: Some applications of laser scanning technology (Leo, 2003)

Image recoding/ printing	Image digitizing	Optical data storage
Color image reproduction	Barcode reading	Phototypesetting
Medical image recording	Optical inspection	Earth resources recording
Data marking and engraving	Confocal microscopy	Data/image display
Micro-image recording	Optical character recognition	Graphic arts camera
Robot vision	Laser radar	Color separation

In laser scanning, various types of tracking and aiming frames and mirrors have been developed to control the laser beam. The aiming frames and mirrors can be generally categorized into two groups - one with rotatable frame and the other with rotatable mirror as shown in Figure 1.1. In a rotatable frame system, the laser mounts on gimbals driven by actuators when tracking and pointing as shown in Figure 1.1. The large inertia of the rotatable frame system results in low bandwidth and slow system response. The rotatable mirror system has been developed to solve these problems (Zhou et al., 2009). In the rotatable mirror system, only the mirror moves, making it much smaller, lighter and therefore faster to respond, greatly increasing the bandwidth of operation.

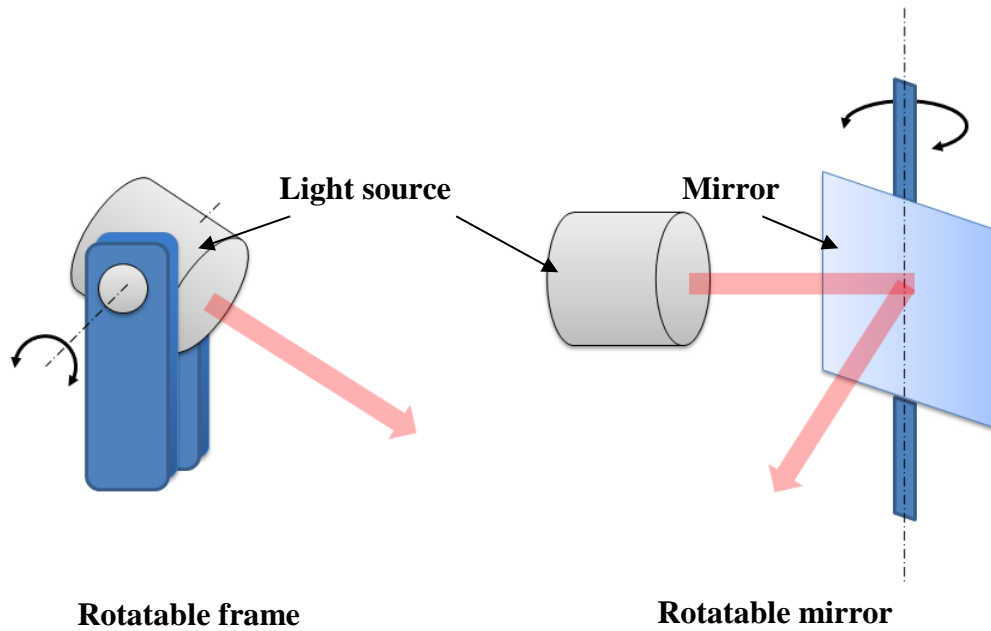


Figure 1.1: Frame forms of tracking and aiming

In the rotatable mirror, the technology is divided into two major groups, namely, 'high inertia' and 'low inertia' (Leo, 2003). The distinction between these scanning technologies is related primarily to the scanning flexibility, i.e. the ability of the scanner to provide repetitive scanning and agile control of the laser beam direction when scanning. There are several advantages of using high inertia scanner such as the ability to provide high regularity scanning, ability to resist instantaneous change in scan speed and to stay in the scan locus when the mirror is oscillated. On the other hand, the low inertia scanner is used for optical scanning applications that require rapid changes in scan speed and high scanning flexibility. The low inertia scanner also enables on-time control and alteration of the scan trajectory path.

The high inertia scanners typically involve motions of significant masses during the oscillation. If the masses are properly balanced, a high inertia scanner can restrain perturbation from the desired scan function. Generally, high inertia scanners can be divided into two families, namely rotational and translational scanners. In the

rotational scanners, three different scanners such as polygons, holographic and oscillatory resonant scanner are found. Those rotational scanners can provide highly ordered data point transfer during scanning. On the other hand, the linear translational scanners can provide high accuracy scanning due to the substantive velocities when travelling in a linear path. Kang et al. (2009) presented a linear translational design that consisted of double-compound leaf spring flexure guide mechanisms actuated by voice coil motor (VCM). The results of 10 nm resolution and 2 mm working range confirmed that the translational component can be employed in precision tracking. Since the present work is not using the linear translational scanner due to the fact of the scanner cannot provide the desired motion function, the details discussion of this scanner mechanism has been excluded.

High inertia scanners are suitable for fine resolution scanning, and thus desired scan function can be achieved. Recently, various applications are using the high inertia scanner in their scan functions. For instance, high-energy laser systems (HEL) (Wehr and Lohr, 1999; Marino and Davis, 2005), free-space optical communications (Xiang et al., 2010), light detection and ranging (lidar) (Liu et al., 2011), semiconductor manufacturing and inspection, laser welding, laser cutting of materials (Du et al., 2011; Urey, 2002), optical data storage, information display (Urey, 2002), scanning optical lithography (Dao and Dentamaro, 2003), and various applications in medical and biomedical systems (Cochran and Vassar, 1990).

The most significant development in the high inertia scanner technology is found to be on the oscillatory resonant scanner due to its ability to achieve large angular displacement and to create near-perfect sinusoidal oscillations. The scanner is named as a resonant scanner because it is driven at resonant frequency. A high Q-factor can be obtained when the scanner is actuated at its resonant frequency. Thus,

the actuation voltage supplied to the system can be reduced while maintaining the desired large scanning angle. According to Chung and Liang (2011), generally portable devices need low operation power consumption. Therefore, operating the scanner in resonant frequency reduced the power consumption, and thus a portable scanner can be obtained. When the resonant scanner is reflecting light to form a linear scanning line, the resonant scanner is renamed as linear optical scanner (LOS) (Xiang et al., 2010). Throughout this thesis, the term 'linear optical scanner' and 'resonant scanner' are used interchangeably.

Scanners used in the oscillatory resonant system can be categorized according to the size of the scanner that is whether the resonant scanner is built in microelectromechanical systems (MEMS) size or large scale size. The large scale based resonant scanner is usually known as the mechanical resonant scanner (MRS). Generally, MEMS can be defined to be chip level devices (usually smaller than 10 mm) which are fabricated using semiconductor, such as silicon (Madou, 2002; Chellappan et al., 2010).

In spite of the reliability of the MEMS based mirror (in resonant scanner) in many technological niches, large size mirror for deflecting the light beam has also drawn the attention of researchers. For instance, barcode scanner broadly used large size mirror (larger than 100 mm²) for automatic information identification. The use of polygon scanners in barcode systems which consist of large components limit the application in highly portable systems (Yaqoob and Riza, 2004). Recently, large size surface-micromachined polysilicon microscanners have been employed for barcode scanning (Duch et al., 2011). However, the convex curvature of the scanning mirrors limits the performance since the curvature causes image distortion when scanning. Moreover, to create a large size MEMS mirror (around 100 mm² or larger), relatively

large die and expensive dry etching equipment for the silicon fabrication is required, thus increasing the production cost (Sasaki et al., 2010; Asada et al., 2000). As explained, the high voltages (above 30 V) for the operation of MEMS electrostatic scanners also limit the portability of the scanner (Yalcinkaya et al., 2007). Besides the application in the barcode scanner, the mechanical resonant scanners are also found in lidar system design. A large mirror is able to reflect larger light spot diameter since larger area of reflection can be achieved. The mirror is needed due to the capability of offering higher optical transmission efficiency, which means that the scanner will have longer detection distance compared to the MEMS scanner. (Xiang et al., 2010; Mu et al., 2008). Thus, a large scale resonant scanner which is able to produce large scanning angle, with a minimum required resonant frequency of 40 Hz and low power consumption is needed for broader spectrum of applications, such as barcode scanner and ultra-short throw projector.

Although resonant scanners are categorized according to their size, i.e. MEMS and large scale, both types of scanners share the same technologies, such as compliant mechanisms and actuation modes. Compliant mechanisms are mechanical devices that provide smooth and controlled motion guidance of the mirror due to the deformation of the compliant components (Todd et al., 2010; Wang and Tai, 2010). Thus, compliant mechanisms (CMs) are used in the optical scanning applications since they have the ability to provide positioning control. CMs do not require sliding, rolling or other types of contact bearings which are often found in rigid mechanisms and actuators. These characteristics enable CMs to achieve reliable, high performance motion control at low cost (Wang and Tai, 2010). Generally, there are several compliant systems available to actuate the resonant scanner, namely flexure hinge, cantilever spring and torsional spring.

In this work, the torsional spring mechanism is used in the design of the large scale resonant scanner due to the limitations found in the flexure hinge and cantilever spring. The design of resonant scanner consists of flexure hinge that will limit the scanner performance due to the undesired parasitic motion error (Awtar and Sen, 2010). Additionally, the angle of deflection is limited by the high degree of constraint (DoC) in the flexure mechanism. Thus, a large angular displacement is restrained when flexure mechanism is used in the scanner (Jong-kyu and Won-kyu, 2011). In a MEMS cantilever spring mechanism scanner designed by Levy and Maaloum (2002) and the large scale cantilever spring mechanism scanner designed by Kheng et al. (2010), a fine control on the beam reflection for the cantilever spring mechanism cannot be achieved because the bending axis is located far away from the mirror as shown in Figure 1.2. Thus, this reason restrained the application of the cantilever spring in the large scale resonant scanner.

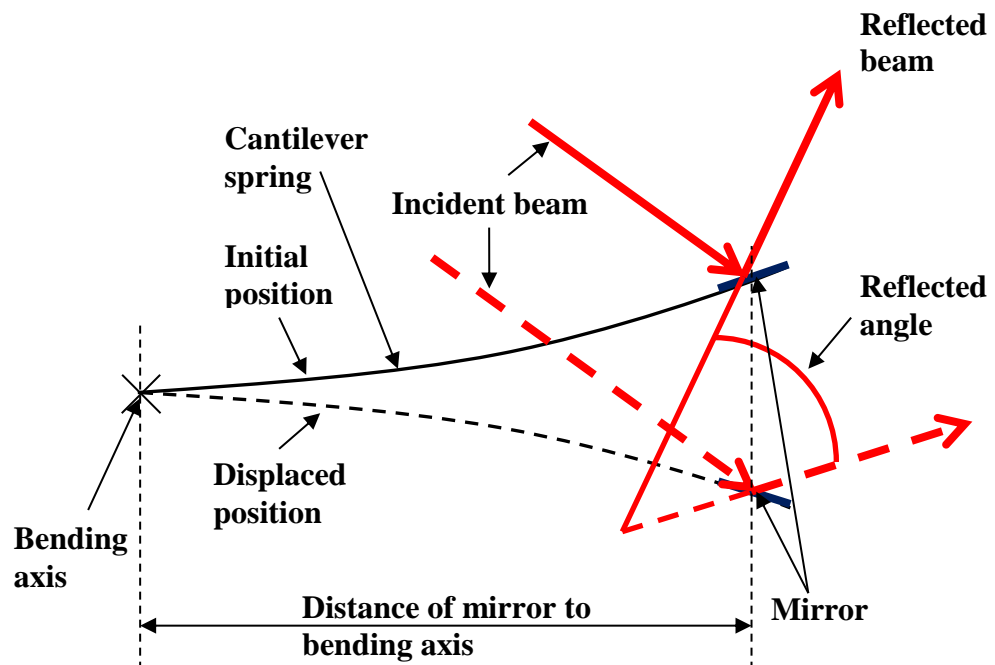


Figure 1.2: Vibration mode of cantilever spring

Various actuators have been designed to actuate the mirror of the resonant scanner. Typically they consist of galvanometric actuator, piezoelectric actuator, or VCM (Xiang et al., 2010). Modern galvanometric positioning actuators work on permanent magnet motor principles (Aylward, 2003). However, galvanometric scanner suffers from some disadvantages, such as high power consumption, and nonlinear distortion caused by the rotational inertia during fast linear scanning (high frequency scanning at uniform scan line and uniform velocity) (Xiang et al., 2010; Qingkun et al., 2008). The piezoelectric effect is employed in scanners that require small displacements with extremely fine resolution (sub-nanometer) or over small travel ranges (several micrometers); the travel range is limited by the dielectric strength and the thickness of the piezoelectric material (Hii et al., 2010). Resonant scanners driven by piezoelectric actuator usually have high resonant frequency, however, they are limited to small deflection angles (Perez-Arancibia et al., 2009). The last compliant structure- VCM can be understood by the components used in traditional electrodynamic loudspeakers, which consist of a coil and a permanent magnet that are joined with the compliant structure. The VCM can deliver large deflection angles and high driving frequency.

According to previous studies, the compliant structure that is commonly used in the design of MEMS resonant scanner is the torsional mechanism. Figure 1.3 shows a MEMS resonant scanner that consists of single crystal silicon. A pair of torsion bar hinges is designed to connect a moving plate to the fixed frame. Then, the moving plate has a driving coil on one surface (backside) and a mirror is attached at the front of the plate (Mu et al., 2008). The torsional spring mechanism plays important role in resonant scanner due to the following advantages:

- To obtain high Q-factor in the oscillation of a resonant scanner, it is desirable to have the torsional mode as the first mode (mode with the lowest frequency) (Urey, 2002).
- If the laser is aimed at the twist axis of the mirror, the incident light impinged and reflected from the mirror is able to maintain at the symmetry axis. Hence, by aiming the laser to the twist axis, fine control of the scanning line can be achieved.
- The torsional spring also helps to reduce power consumption due to the inherent restoring force.

Although the MEMS and large scale scanners share the same technology in compliant structure and actuators, the use of torsional spring mechanism and VCM in the large scale resonant scanner for large size mirror and large scanning angle has not been investigated in the past. Thus, the investigation on the design for torsional spring mechanism and VCM is necessary in this research work.

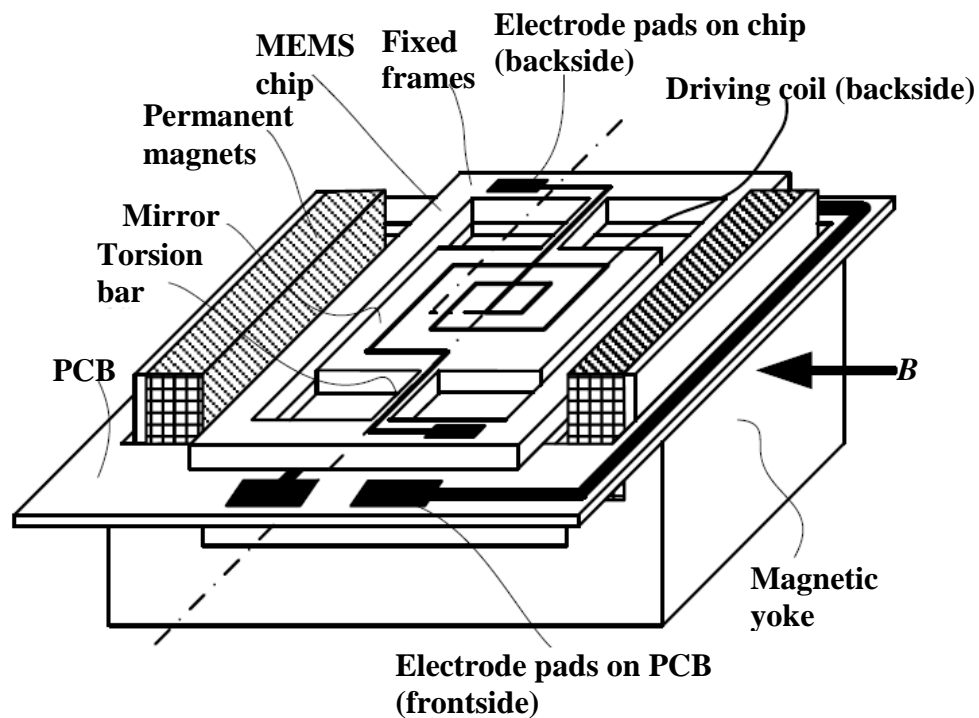


Figure 1.3: Typical MEMS torsional scanner (Mu et al., 2008)

Besides the design of the complaint structure and the VCM, damping characteristic of the scanner was presented in this research work because damping is one of the limiting factors for the reachable maximum scanning angle. The study of damping characteristic becomes an important issue in the context of resonant scanner. Hao et al. (2002) presented a mathematical model to predict the squeeze-film damping effect in a MEMS 2D tilt mirror. Jana and Raman (2010) studied the characteristic of surrounding fluid on a micro-resonant scanner based on Reynolds equations and concluded that viscous damping is an essential damping model in torsional scanner. In these papers, the authors only concentrated on the squeeze-film damping effect that occurs at close proximity gaps found in MEMS resonant scanner. Hence, the damping study on the large scale resonant scanner has yet to be carried out. Furthermore, the presence of viscous damping in large scale resonant scanner is not well explored in these papers. Also, the damping effect considered in those studies is constrained only at the equilibrium position, which is amplitude independent study. Finally, the nonlinearities in damping behavior have been neglected. Hence, the characteristic study of the damping behavior of the large scale resonant scanner is necessary.

The resonant behavior of linear optical scanner is a very useful dynamic characteristic for maximizing the scanning angle (Wang et al., 2007). For instance, the scanning angle of the torsional spring scanner and the cantilever spring scanner (Kheng et al., 2010) are significantly increased when actuated at the resonant frequency. However, the resonant frequency of large scale resonant scanners can vary due to the following factors:

- The scanner's resonant frequency is very sensitive to the manufacturing variation, such as the inconsistency of product dimensions and the mass variation (Liu et al., 1997; Cole and Ahn, 2002).
- Although the larger inertia large scale resonant scanner are inherently resistant to the frequency perturbation, the resonance behavior for the large scale resonant scanners experiences minor frequency variation due to the environmental conditions (Perez-Arancibia et al., 2009; Orzechowski et al., 2008).
- The resonant frequency will also vary in time due to the fatigue effect, whereby the resonant frequency decreases when crack propagation occurs (Kheng et al., 2010).
- The resonant frequency of a scanner will also vary under different operating conditions such as driving voltages and inductance voltages (Kaajakari et al., 2005; Anac and Basdogan, 2008).

The phenomenon of frequency variation poses critical performance limitations, and even small variation in scanning angle often produces significant deviation due to the amplification by the optical path length (throw distance) (Qingkun et al., 2008). Therefore, it is necessary to tune the driving frequency of the actuator due to the frequency variation.

The torsional resonant scanner exhibits an interesting dynamic behavior, namely hysterical frequency response. When the driving frequency of the actuator is increased from lower frequency to a higher frequency (swept up), the scanning angle obtained will be several times larger than that of the swept down from the higher frequency to the lower frequency. This dynamic characteristic (hysterical frequency response) has been studied for torsional MEMS resonant scanner since 1998 (Turner et al., 1998). However, the effect between the hysterical frequencies on the scanning

angle for large scale torsional scanner has not been reported to date. Hence, it is desirable to study on the variation of scanning angle for large scale torsional resonant scanner when the drive frequency is swept up or swept down.

1.1 Problem statement

One of the goals that optical researchers are currently pursuing is to design a resonant scanner that has large-size mirror, large scanning angle and low power consumption for portable applications such as barcode scanner, lidar and many others. The existing polygon scanner plays an important role in barcode scanning. However, the bulky mirror and discontinuity in the scanning mirror limits the scanner performance. In the previous work presented by Kheng et al. (2010), a cantilever spring mechanism large size linear optical scanner (LOS) was proposed. However, the bending mode of the spring oscillation cannot provide a constant locus for laser aiming because the bending axis is located behind the mirror. Thus, timing control on the scan line cannot be achieved. In view of that, a novel large size torsional resonant scanner is needed to be developed.

Recently, the damping behavior of the MEMS linear optical scanner (LOS) has been studied by researchers especially on the squeeze-film damping effect. However, the presence of viscous damping in the large size torsional scanner is assumed to be insignificant. Also, they concentrated only on the damping effect at the equilibrium position which consists of a non-amplitude dependent study and the nonlinearities damping behavior are ignored in their studies. To counter this limitation, a study to find the dependency of viscous damping on scanning angle in a large size torsional resonant scanner based on the free response profile of LOS is desired. In the real world, environmental perturbation will contribute to damping

variation of the LOS. Therefore, the investigation on the effects of pressure variations and various couplings for the LOS to the damping behavior of LOS is necessary. Also, a nonlinear damping ratio study is needed to understand the dynamic behavior of the LOS.

The determination of the resonant frequency for scanners has drawn the attention of researchers since operating the scanners at resonant frequency will provide maximum scanning angle and reduce the power consumption. Previously, the study on MEMS torsional resonant scanners was the main thrust in optical systems. Therefore, the tracking of resonant frequency for large size torsional resonant scanner was not reported to date. Besides, the hysterical frequency response on the large size torsional resonant scanner was also neglected. Thus, a detailed study of the frequency responses of the large size torsional resonant scanner is necessary for attaining maximum scanning angle.

1.2 Objectives

The main objectives of this research are as follows:

- To design and develop a large size torsional spring mechanism based on resonant scanner that can provide the required minimum resonant frequency (above 40 Hz).
- To investigate the electromagnetic characteristics of the voice coil motor in the resonant scanner for various magnet positions.
- To characterize the damping behavior of the large size torsional spring mechanism resonant scanner based on the nonlinear damping ratio model.

- To design test algorithms of the controller for resonant frequency tracking and analyze the hysterical frequency response of the large size torsional spring mechanism resonant scanner for maximum scanning angle.
- To verify the performance of the large size resonant scanner under frequency perturbation.

1.3 Scope of study

This research work involves the design, improvement, and evaluation of a scanner based on the resonant frequency, scanning angle, power consumption, and the consistency interval for the images. The consistency of the images is obtained based on the length measurement of each scanning line. However, a specific application of this scanner will not be included, since the objective of this research work is merely constrained to the development and analysis of the novel large scale resonant scanner.

The linear optical scanner (LOS) design requirements contradict each other. For instance, to increase the resonant frequency the stiffness of torsional spring needs to be increased. However, increasing the stiffness of the torsional spring will lead to a decrease in the scanning angle, and thus decreasing the LOS performance. Conversely, in order to increase the scanning angle, the stiffness of the torsional spring needs to be decreased. To maximize the scanning angle, the magnetic forces produced from the VCM should be increased, but this would increase the power consumption. Thus, it is a challenge to find a compromise among the design requirements.

The mechanical design studies were only conducted on the optical systems (torsional spring, suspended plate and magnet position) of the LOS. However, the

holding structure (holder) was ignored due to the assumption of high rigidity of the structure in comparison to the optical systems.

Since the aim of this research work involved the design of large scale torsional spring mechanism resonant scanner, an overall study on mechanical design, damping characteristic, electromagnetic study, and rule-based control design were conducted merely for the performance testing. This research work involves several fields of studies, thus the depth of study on each field is merely confined to the large scale torsional spring mechanism resonant scanner.

1.4 Thesis outline

The thesis is arranged as follows. Chapter 1 described the introduction of the research, problem statement and objectives. The linear optical scanners in the published literatures as well as the commercially available scanners are reviewed in Chapter 2 according to the functional components: compliant mechanisms, actuators and controller. The advantages and limitations of the available scanners are discussed in detail.

The chapters are arranged according to the functional components design except Chapter 5 which presents the study on the damping characteristic. In Chapter 3, a study on the geometry of the compliant mechanism (torsional spring) is described. The dimensions of the torsional spring: width, length, and thickness are optimized using finite element analysis (FEA) to find the relationship among the design requirements. Then, an experimental validation is performed based on the resonant frequency of the linear optical scanner (LOS). The main aim of this chapter is to determine the dimensions of the torsional spring that can provide a reasonable life span while attaining the design requirements. To increase the angular

displacement of the LOS, the magnetic forces produced from the VCM must be maximized. Thus, VCM development and the effect of magnet position on the LOS are presented in Chapter 4. An analytical study was conducted on the relationship between magnetic forces and magnet to coil distance which was presented in Chapter 4 as well. Several VCMs were fabricated based on the number of coil turning and various coil dimensions for analytical-experimental validation. Then, a voice coil motor which has maximum magnetic force was selected as the actuator for the linear optical scanner.

To investigate the damping characteristic of the linear optical scanner (LOS), a nonlinear damping ratio model is discussed in Chapter 5. The model is able to predict the variation of angular displacement at the free response profile of LOS. Several operating conditions are proposed for experimental testing and validation. Thus, the relationship between the damping behavior and the scanning angle was obtained. In Chapter 6, the testing algorithms of the LOS are presented. Several algorithms were developed for the resonant frequency tracking and hysterical frequency response tracking. The free response profile of the LOS is employed for the resonant frequency tracking algorithm, where the period of the free underdamped vibration is recorded with interruption function. Performance testing on the constant scanning line and the ability of the resonant frequency tracking are described in Chapter 6 as well. Meanwhile, the results and discussion of each chapter have been embedded within each chapter. A summary of individual chapter will be presented in each chapter as well. Therefore, a chapter that presents the detailed results and discussion will not be presented. However, the conclusions of the research are drawn in Chapter 7. Recommendation and suggestions are provided for future work in the same chapter.

CHAPTER 2 LITERATURE REVIEW

2.0 Introduction

To illustrate the overview of this chapter, a tree diagram is shown in Figure 2.1. Literature survey on the linear optical scanner (LOS) with emphasis on the functional components of scanner will be presented according to the associated actuation principles, compliant structure, control system and damping characteristics. However, before discussing the linear optical scanner according to the functional components, a concise overview of the scanner technology is presented.

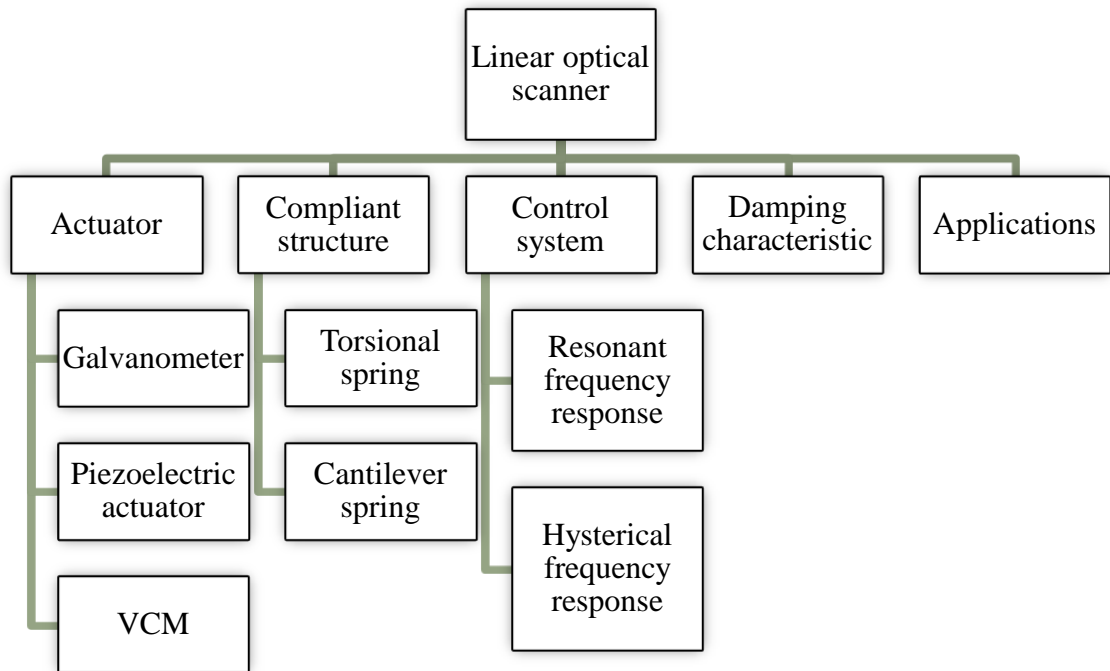


Figure 2.1: Overview of literature review

Various designs and practices that have been researched upon and developed in the past for the linear optical scanner (LOS) are reviewed in this chapter. Since the review is separated according to the functional components, the advantages and the disadvantages of each component will be discussed. Special

attention will be given to recently published research works which are relevant to the LOSs.

2.1 Overview of optical scanning technology

According to the classification carried out by Leo (2003), oscillatory resonant scanners are grouped into high inertia rotational scanners, which is in the same domain as the rotational polygonal scanners and holographic scanners as shown in Figure 2.2. Oscillatory resonant scanner is categorized in this group because of the unique characteristic of showing the high inertia scanning properties although the rotor in the resonant scanner may actually consist of low moment of inertia structures. Typically, high-inertia scanning should involve significant mass motion. However, when actuated at resonant frequency, the resonant scanner provides the behavior of disallowing rapid stop or alteration in the frequency and motion, unless environment perturbations are imposed (Orzechowski et al., 2008). Thus, the resonant scanner is categorized under the mentioned group: high inertia rotational scanner.

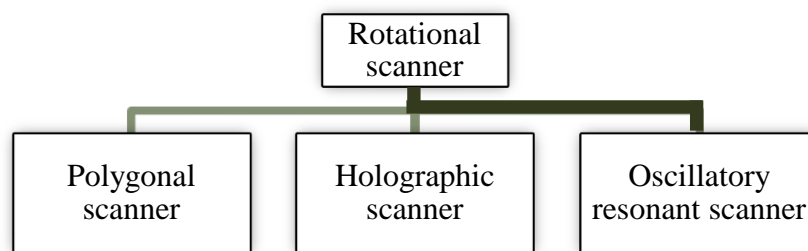


Figure 2.2: Classification of rotational scanner (Leo, 2003)

2.1.1 Polygonal scanner

Polygonal scanner uses a rotating polygon mirror accompanied by the external focused light source such as laser for scanning application (Yasseen et al.,

1999; Kim et al., 2008). Rotating polygonal scanner can be classified into two main configurations: pyramidal polygon and prismatic polygon as shown in Figure 2.3. The pyramidal polygon reflects the incident light beam (laser) which is parallel to the rotating axis. The pyramidal polygon scanners operate in radial symmetry and reflect the laser through a scanning angle which is same as mechanical angular displacement of the rotating mirror as shown in Figure 2.3. Thus, the magnification factor of the mirror reflection is 1 for pyramidal polygon. The prismatic polygon scanner has a magnification factor of 2, since the scanning angle obtained is twice of the mechanical angular displacement when the laser is illuminated in the same x - z plane as shown in Figure 2.3 (Leo, 2003).

Polygonal scanners are used in diverse areas of light dispersion application, such as barcode reading, image digitization, printing, data storage, confocal microscopy, and manufacturing quality inspection. The polygonal scanners are able to provide a high scanning angle (up to 110°) depending on the number of facets employed (Yasseen et al., 1999). The scanners offer high duty cycle (time efficiency) for the scanning process especially for the monogon scanner (Leo, 2003). The lower numbers of the facets give higher duty cycle. The duty cycle η can be defined as the ratio of the active portion to the full scan period, and can be expressed as (Leo, 2003),

$$\eta = 1 - \frac{\tau}{T} \quad (2.1)$$

where, τ is the blanking time and T is the full scan period.

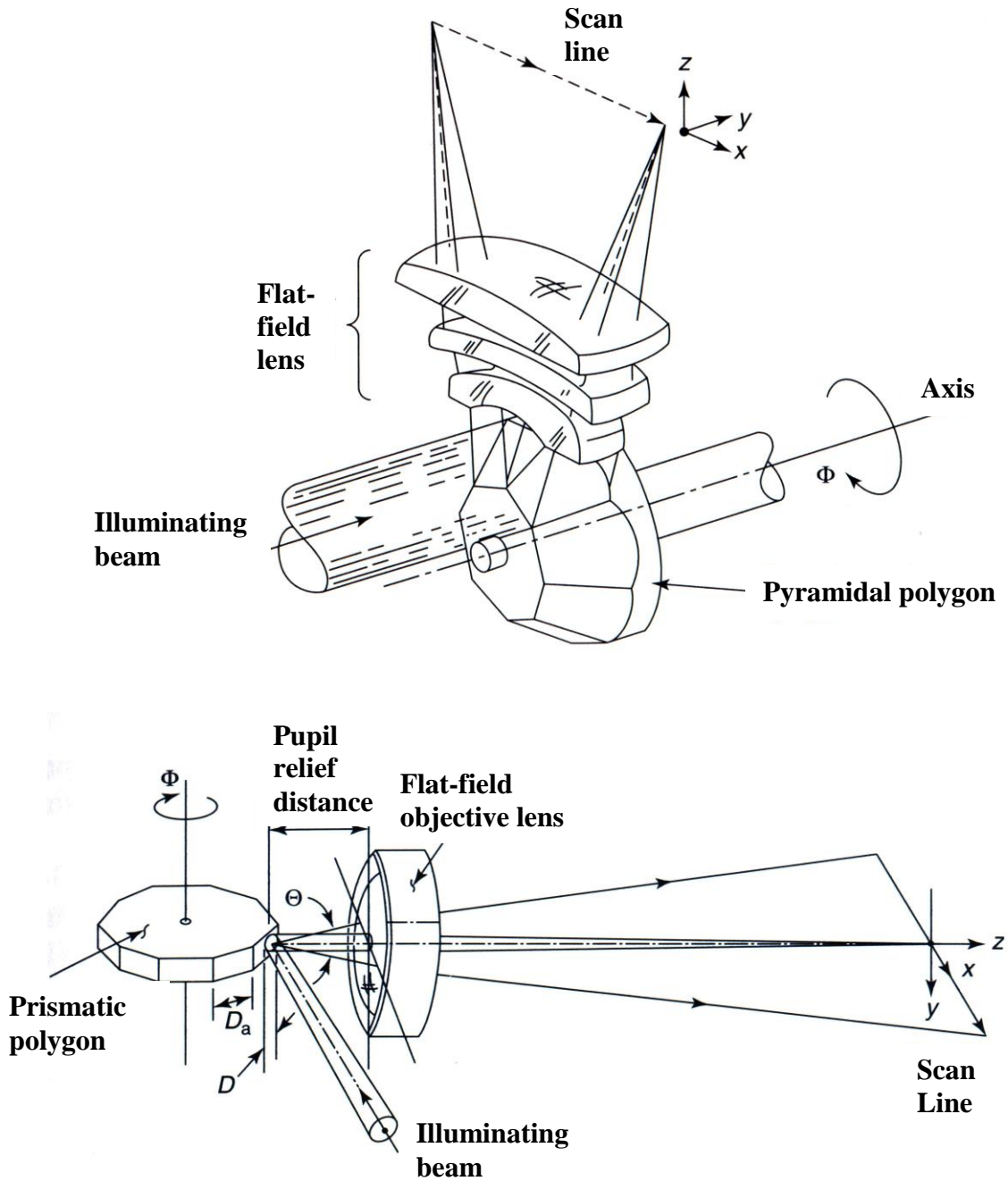


Figure 2.3: Pyramidal polygon and prismatic polygon (Leo, 2003)

However, when the number of facets (mirrors) of the polygon increases, the number of straddle mirrors increases. Thus, the portions of the active scanning period are reduced over the full scan period due to the scan discontinuities (Aylward, 2003). In other words, the connection lines among the mirror increases when the number of facet increases. Once the light beam (laser) is aimed on the connection lines, the

reflected beam is diffused instead of reflected, and thus the active scanning period decreases. Another concern of using the polygonal scanners are these scanners create abnormal noise and vibration due to the mechanical contact between the rotating shaft and the stationary sleeve (Kim et al., 2008). Jung et al. (2009) developed a finite element method for the polygonal scanner to study the flexibility of rotation. They studied the mechanical resonant vibration due to the mass imbalance when rotation. In most of the past works the researchers studied only the causes for the mechanical vibration. However, to date, the presence of noise and vibration has not been solved completely in high speed scanning applications (Jung et al., 2011). The detailed study on the presence of noise and vibration for the polygonal scanner is not included since the polygonal scanner is not used in this research work.

2.1.2 Holographic scanner

Since holographic scanners are categorized under the same group with the polygonal scanners, they share some similar operation disciplines, such as the holographic components are rotated about an axis as shown in Figure 2.4. In short, the polygon mirror of the polygonal scanner is replaced by a holographic deflector (Rowe, 1997). The holographic deflector consists of an array of diffractive elements disposed about the periphery of a substrate, to serve as transmissive or reflective facets (Leo, 2003). The holographic element materials can be divided into three large groups according to their applications: holographic emulsions, dichromated gelatins, and photoactive polymers (Blaya et al., 2001). After the invention of holography by Gabor (1948), the holography technology plays crucial roles in many applications. For example, holographic optical elements, scanners, optical disc systems, optical computing, holographic displays and integrated optics have been developed.

However, there are some advantages and limitations of using holographic scanners for imaging or scanning in comparison with polygonal scanners.

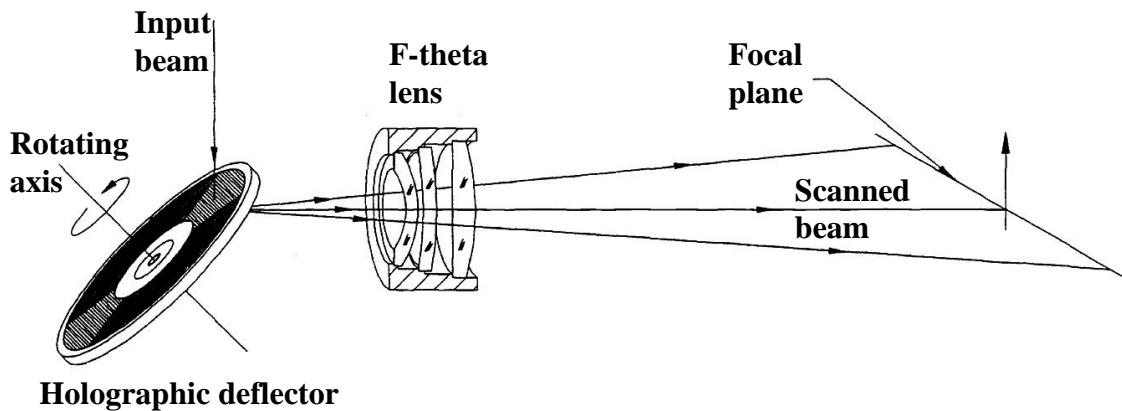


Figure 2.4: Typical holographic scanner (Rowe, 1997)

The scanning discontinuities found in polygonal scanners can be eliminated with the replacement of polygon mirrors with the holographic deflector since the mirror connection lines are eliminated. The aerodynamic loading and the windage can be reduced by the holographic deflector which provides smooth substrate surface (Rowe, 1997). When operating the facets in the Bragg regime, beam misplacement due to the shaft wobble can be reduced significantly. Bragg regime is defined to be a regime where the transmitted waves and diffracted waves are present simultaneously when the diffractive substance is illuminated with a focused light (Moharam et al., 1980; Liu et al., 2011).

Although the holographic scanners are able to provide various advantages, but the design, fabrication, and testing requires unique technical discipline (Leo, 2003; Bhatt et al., 2008). Thus, holographic scanners often incurred significant design investment. The f-theta lens assembly found in holographic scanners is often the most expensive component in the holographic scanners. Thus, a curve mirror was introduced as a replacement of f-theta lens in order to reduce the cost of fabrication

(Rowe, 1997). However, if the f-theta lens is replaced, the scanner will lose the functionality of the f-theta lens in line bow correction, field flattening, and linearity correction (Leo, 2003). Therefore, the performance will deteriorate with the replacement of curve mirror in holographic scanners. Since the holographic scanners are based on the diffraction concept, the transmission efficiency is lower compared to reflector based scanner. Hence, the holographic scanners often have shorter detection distance in comparison with the reflector based scanner (Xiang et al., 2010).

2.1.3 Oscillatory resonant scanner

The scanning non-uniformities arising from the rotating polygon mirrors and the low duty cycle of the holographic deflectors can be eliminated by the replacement of one facet (mirror). Oscillatory (vibrational) scanners involve the changing of multiple mirror into single mirror as shown in Figure 2.5 (Leo, 2003). The mirror of the oscillatory resonant scanner is mounted in the position coincident with the rotating axis as shown in Figure 2.5(b). With this orientation, the plane of the input and output incident light beam is positioned in the perpendicular configuration to the oscillating axis. When the incident light is aimed at the oscillating axis, the scanning angle obtained is twice that of the mechanical angular displacement (magnification factor of 2). Since the mirror is oscillated instead of rotated through a full cycle, the blanking time can be eliminated, and thus continuity in scanning and high duty cycle can be obtained. Although the inertia of the facet is low, allowing high cyclic rates, but the resonant scanner allows no random access on the oscillating displacement. Thus, fine control can be obtained on the sinusoidal displacement profile for the scanner (Leo, 2003).

Typically, there are several types of oscillatory resonant scanners that are commonly found in the literatures. They include galvanometric (Aylward, 2003), resonant scanners, and piezoelectrically driven mirror transducers (Perez-Arancibia et al., 2009). Although the resonant scanner can be divided into two major groups according to the size of the scanner (MEMS or large scale), the main differences between these oscillatory resonant scanners are the actuation modes used and the compliant structures in actuating the mirror. Therefore, in the following paragraphs the literature is reviewed according to functional components comprising actuator, compliant mechanism and control system of the scanner.

Apart from those functional components, the damping characteristic studies performed by researchers will be discussed after these reviews. The damping characteristic is a significant limiting factor on the scanning angle of the scanner, and thus it becomes a crucial element in scanner performance studies. To achieve the resonant frequency, each of these scanners must be controlled by a testing algorithm. The testing algorithm will ensure that the driving frequency of the actuators is maintained at the changed resonant frequency when frequency perturbations are imposed. Thus, a review on the characteristic of the resonant frequency including the hysterical frequency response of the torsional scanner will be discussed as well. Then, the applications of LOS will be presented in the last section of this chapter.